Clinical Translational Research

Oncology

Oncology 2013;84:362–370
DOI: 10.1159/000348884

Received: November 26, 2012
Accepted after revision: February 13, 2013
Published online: May 15, 2013

Intracellular ATP-Binding Cassette Transporter A3 is Expressed in Lung Cancer Cells and Modulates Susceptibility to Cisplatin and Paclitaxel

Tobias R. Overbeck[a] Timo Hupfeld[a] Doris Krause[a]
Regina Waldmann-Beushausen[b] Bjoern Chapuy[a] Bjoern Güldenzoph[a]
Thiha Aung[a] Nobuya Inagaki[c] Friedrich A. Schöndube[b] Bernhard C. Danner[b]
Lorenz Truemper[a] Gerald G. Wulf[a]

Departments of [a]Hematology and Oncology and [b]Thoracic and Cardiovascular Surgery, University Medical Center Göttingen, Göttingen, Germany; [c]Department of Diabetes and Clinical Nutrition, Graduate School of Medicine, Kyoto University, Kyoto, Japan

Key Words
ABCA3 · ATP-binding cassette transporter · Cisplatin · Drug resistance · Lung cancer · Paclitaxel

Abstract
Patients with advanced-stage bronchial cancer benefit from systemic cytostatic therapy, in particular from regimens integrating cisplatin and taxanes. However, eventual disease progression leads to a fatal outcome in most cases, originating from tumor cells resisting chemotherapy. We here show that the intracellular ATP-binding cassette transporter A3 (ABCA3), previously recognized as critical for the secretion of surfactant components from type 2 pneumocytes, is expressed in non-small-cell lung cancer (NSCLC) cells. With some heterogeneity in a given specimen, expression levels detected immunohistochemically in primary cancer tissue were highest in adenocarcinomas and lowest in small cell lung cancers. Genetic silencing of ABCA3 in the NSCLC cell line models A549, NCI-H1650 and NCI-H1975 significantly increased tumor cell susceptibility to the cytostatic effects of both cisplatin (in all cell lines) and paclitaxel (in two of three cell lines). Taken together, ABCA3 emerges as a modulator of NSCLC cell susceptibility to cytostatic therapy.

Introduction

Despite improvements in diagnostics and therapy, 5-year overall survival rates of patients with lung cancer remain bleak (15–18%) [1]. In patients without metastatic involvement, multidisciplinary approaches including surgery, radiotherapy and chemotherapy can achieve cure for some patients. For patients with metastatic disease, representing 40% of all patients at primary diagnosis [2], transient control of cancer growth can only be provided by systemic cytostatic treatment regimens. Within such regimens, combinations of vinca alkaloids, anthracyclines, topoisomerase inhibitors, antimetabolites and DNA alkylating drugs have shown activity against lung cancer, with limited promising results obtained with combination protocols integrating platinum derivatives and taxanes for patients with non-small-cell lung cancer (NSCLC) and platinum combined with etoposide in small-cell lung cancer (SCLC) patients [1]. Thus, as current standard of care, platinum-based combination chemotherapy has generated a plateau in the overall response rate of about 25–35% in the first-line treatment of stage-IV NSCLC patients [3]. In patients who experience primary progress or relapse of disease, tumor regrowth must

KARGER

0030–2414/13/0846–0362$38.00/0

E-Mail karger@karger.com
www.karger.com/ocl

Tobias R. Overbeck, MD
Department of Hematology and Oncology
University Medical Center, Robert-Koch-Strasse 40
DE–37075 Göttingen (Germany)
E-Mail tobias.overbeck@med.uni-goettingen.de

originate from cells resisting chemotherapy, and several mechanisms protecting lung cancer cells from cytostatic effects have been described, ranging from impaired apoptosis induction and tumor dormancy to classical multidrug resistance and cellular drug extrusion by drug-transporting proteins such as ATP-binding cassette (ABC) transporters and lung resistance protein [4–12].

Analyzing the intrinsic drug efflux capacity pertinent to leukemic progenitor cells with the side population phenotype, we previously detected a specific role for the ABC transporter A3 (ABCA3) in drug resistance of myeloid leukemia as well as neuroblastoma stem cells [13–15]. Genetic manipulation studies clearly established an association of ABCA3 expression with drug resistance, and the intracellular localization of ABCA3 in the membranes of lysosome-related organelles led to the discovery of ABCA3-mediated lysosomal drug sequestration as a contributing mechanism [16, 17]. Intriguingly, ABCA3 has previously been described as a key regulating transport protein in the process of surfactant extrusion into the pulmonary alveolae [18, 19]. Children with functional relevant mutations in the ABCA3 gene experience severe respiratory distress syndrome after birth, and experimental study of surfactant biogenesis revealed a critical role of ABCA3 function for the amount and composition of phospholipids in the vesicular transport of cytoplasmic multilamellar bodies of type 2 pneumocytes to the multitrabecular bodies carrying the surfactant into the alveolae [20–22]. With type 2 pneumocytes as the major cells of physiological ABCA3 expression as well as the transporter function in vesicular transport and secretion, we here addressed ABCA3 expression in transformed bronchoepithelial cells and its role in the secretion of the cytostatic drugs most commonly used in lung cancer therapy.

Materials and Methods

Cell Culture, Lentiviral Transfection and ABCA3 Detection

The human lung cancer cell lines A549 [23], NCI-H1650 [24] and NCI-H1975 [24] as well as the SCLC cell line NCI-H69 [25] were propagated in RPMI 1640. HEK293T cells were grown in DMEM. The stable ABCA3-eGFP and eGFP transfectants HEK293/ABCA3-eGFP and HEK293-eGFP described previously [17] were routinely cultured in DMEM supplemented with 300 μg/ml G418 (Carl Roth, Karlsruhe, Germany). All media were supplemented with 10% heat-inactivated fetal calf serum (Gibco-BRL, Karlsruhe, Germany), penicillin/streptomycin (Sigma-Aldrich Chemie, Steinheim, Germany/Biochrom, Berlin, Germany) and GlutaMAX I (Gibco-BRL). For shRNA-mediated silencing of ABCA3 in the lung cancer cell lines, two validated specific shRNA sequences [the RNAi Consortium, www.broadinstitute.org/rnai/trc: TRC clone ID TRCN0000059338, here referred to as shABCA3.38: forward 5′-CCGG(GCCCAGCTCATTGGGAAATTT)CTCGAG(AAATTTCCCAATGAGCTGGGC)TTTTTG-3′ and reverse 5′-AATTCAAAAA(AAATTTCCCAATGAGCTGGGC)CTCGAG(GCCCAGCTCATTGGGAAATTT)-3′, and TRC clone ID TRCN0000059339, here referred to as shABCA3.39: forward 5′-CCGGGCCCAGCTCATTGGGAAATTTCTCGAGAAATTTCCCAATGAGCTGGGCTTTTTG-3′ and reverse 5′-AATTCAAAAAGCCCAGCTCATTGGGAAATTTCTCGAGAAATTTCCCAATGAGCTGGGC-3′] were cloned into pLKO.1-eGFP (Addgene, Cambridge, Mass., USA) and lentiviral particles produced in the HEK293T producer cell line with the plasmids pCMV-ΔR8.91 (containing gag, pol and rev genes) and pMD.G (VSV-G-expressing plasmid), as previously reported [26]. Selection was performed using puromycin. Cells were cultured without puromycin 7 days before viability assays. Stable ABCA3 knockdown cell lines, i.e. A549^{shABCA3}, NCI-H1650^{shABCA3} and NCI-H1975^{shABCA3} were propagated like the corresponding wild-type cell lines as described above. Expression of the lentiviral construct was determined by flow-cytometric evaluation of eGFP, and only samples exceeding 90% marker expression were used in further experiments. For ABCA3 detection in in vitro propagated cell populations, we performed indirect immunocytology (dilution 1:200) following cytocentrifugation as well as Western blot (dilution 1:500) of whole-cell lysates as described before, either using a primary polyclonal rabbit antibody against human ABCA3 or a commercially available monoclonal rabbit antibody to ABCA3 (HPA007884; Sigma-Aldrich Chemie) [16, 17, 19, 27].

Immunohistochemistry

The human lung cancer tissue microarray (TMA) LC2001 was obtained from a commercial tissue bank (US Biomax Inc., Rockville, Md., USA). Clinical information on the 187 patients with lung cancer (TMA) is summarized in table 1. All samples were achieved by surgery of the primary tumor before any treatment. Outcome data were not available in this cohort. The mean age of the patients was 56.4 ± 8.2 years (range 30–78). Histological subtypes of lung cancer were adenocarcinoma, squamous cell carcinoma, SCLC, carcinoid and mucoepidermoid carcinoma at the following percentages: 33.2, 42.2, 12.8, 7.5 and 4.3%, respectively. Pathological staging of these patients was performed according to the 6th edition of the International System for Staging Lung Cancer [28]. Immunohistochemistry was performed using the primary antibody to ABCA3 (HPA007884; Sigma-Aldrich Chemie) diluted 1:150 in AK diluent (Dako, Hamburg, Germany) and stained following standard protocols [17]. Secondary antibody (AP anti-rabbit polymer; Zytomed Systems, Berlin, Germany) was visualized using liquid permanent red chromogen in liquid permanent red chromogen substrate buffer (Dako). ABCA3 cytoplasmic intensity staining levels were analyzed by panel agreement of two independent reviewers as negative, weak, intermediate or strongly positive. The proportion of positive tumor in relation to the whole tumor was determined in percent. Normal epithelial lung tissue adjacent to the tumor area as well as 8 tissue samples of normal lung tissue (LC2001) were used as positive (type 2 pneumocytes) and negative controls.

Viability Assays and Statistical Evaluation

Cell sensitivity to cytostatic drugs was determined using the 3-(4,5-dimethylthiazol-2-yl)-2,5-diphenyltetrazolium bromide (MTT) assay, as previously described [17]. Cells were seeded in triplicate in 96-well culture plates at a density of 1×10^5 cells/well

Table 1. Characteristics and staging of 187 patients (TMA LC2001)

Mean age ± standard deviation, years	56.4±8.2	
Range	30–78	
All patients	187	100.0%
Gender		
Female	57	30.5%
Male	130	69.5%
Histological subtype		
Adenocarcinoma	62	33.2%
Squamous cell carcinoma	79	42.2%
SCLC	24	12.8%
Carcinoid	14	7.5%
Mucoepidermoid carcinoma	8	4.3%
Grading		
I	11	5.9%
II	77	41.2%
III	72	38.5%
Unknown	27	14.4%
pT status		
T1	33	17.6%
T2	120	64.2%
T3	29	15.5%
T4	5	2.7%
pN status		
N0	131	70.1%
N1	38	20.3%
N2	17	9.1%
N3	1	0.5%
Pathological stage (UICC, 6th edition)		
I	119	63.6%
II	37	19.8%
IIIa	25	13.4%
IIIb	5	2.7%
IV	1	0.5%

Numbers (%) of patients are shown except for age.

and were treated with the indicated concentrations of cisplatin (Teva, Ulm, Germany), vinorelbine (Pierre Fabre Pharma, Freiburg, Germany) and paclitaxel (Teva) for 3 h each, washed and then incubated for a period of 24 h. After 24 h at 37°C, the culture volume of 100 µl was supplemented with MTT in phosphate-buffered saline to achieve a final concentration of 0.5 mg/ml. After a 4-hour incubation, the supernatant was discarded, and adherent cells resuspended in 30% (v/v) dimethyl sulfoxide, 5% (v/v) formic acid and 1% (w/v) Triton X-100 (all from Sigma) dissolved in isopropanol. Light absorbance from formazan was measured at 540 nm on a Tecan SLT photometer (Tecan SLT Spectra). We expressed the effect on viability as the ratio of values from treated samples with wild-type ABCA3 versus the knockdown variant. EC_{50} was defined as the concentration of drug causing a 50% inhibition of cell growth in wild-type cells compared with knockdown variants.

To estimate differences between cohorts of samples with and without experimental intervention, two-way ANOVA with a Bonferroni post hoc test was applied, with differences of $p < 0.05$ considered significant.

Results

Expression of ABCA3 in Lung Cancer Cells

The physiological expression of ABCA3 in specialized alveolar cells had raised our interest for the prevalence and intratumoral expression pattern of the ABC transporter in transformed pulmonary cells. First, we analyzed 187 cases of primary lung cancer for ABCA3 protein expression in a TMA representing all major types of epithelial lung cancer tumors. Whereas we found no or only very low levels of ABCA3 in small fractions of cells in SCLC tissues, the majority of cancers with non-small cell differentiation showed significant expression of the ABCA3 transporter protein (fig. 1; table 2). Within the NSCLC, expression patterns varied, ranging from >75% strongly positive cells in some cases of adenocarcinoma to low-level expression in cases of predominant squamous cell differentiation (fig. 1; table 3). Of note, intratumoral expression patterns were heterogeneous in all histological subtypes, with subfractions of cells displaying higher amounts of the ABCA3 transporter (table 3).

With respect to subgroups as gender, grading, pT/N status or pathological stage, there were no major differences in the two groups of staining intensity (negative/weak and intermediate/strong) except for the histological subtype (table 2).

In NSCLC, we found cytoplasmic expression of the transporter in all three cell lines tested, which was comparable to the level obtained by ectopically enforced expression in HEK293 cell lines (fig. 2a). In contrast to the NSCLC cell lines, the SCLC cell line NCI-H69 showed no expression of ABCA3 (fig. 2a).

The intracellular staining pattern, with ABCA3 being organized in cytoplasmic vesicular structures, was reminiscent of the staining profile of ABCA3 previously found in other malignancies [15, 17]. Thus ABCA3 is expressed in the majority of NSCLC samples with remarkable inter- and intratumoral heterogeneity.

Role of ABCA3 in the Susceptibility of Lung Cancer Cell Lines to Cisplatin and Paclitaxel

Our previous findings associated ABCA3 expression with leukemia cell resistance against anthracyclines and vinca alkaloids. Therefore, we assessed to which extent ABCA3 protects lung cancer cells against the cytostatic effects of drugs typically applied to control disease in lung cancer patients, i.e. cisplatin and paclitaxel. Thus, we exposed the lung cancer cell lines A549, NCI-H1650, NCI-H1975 and their knockdown variants to cisplatin, pacli-

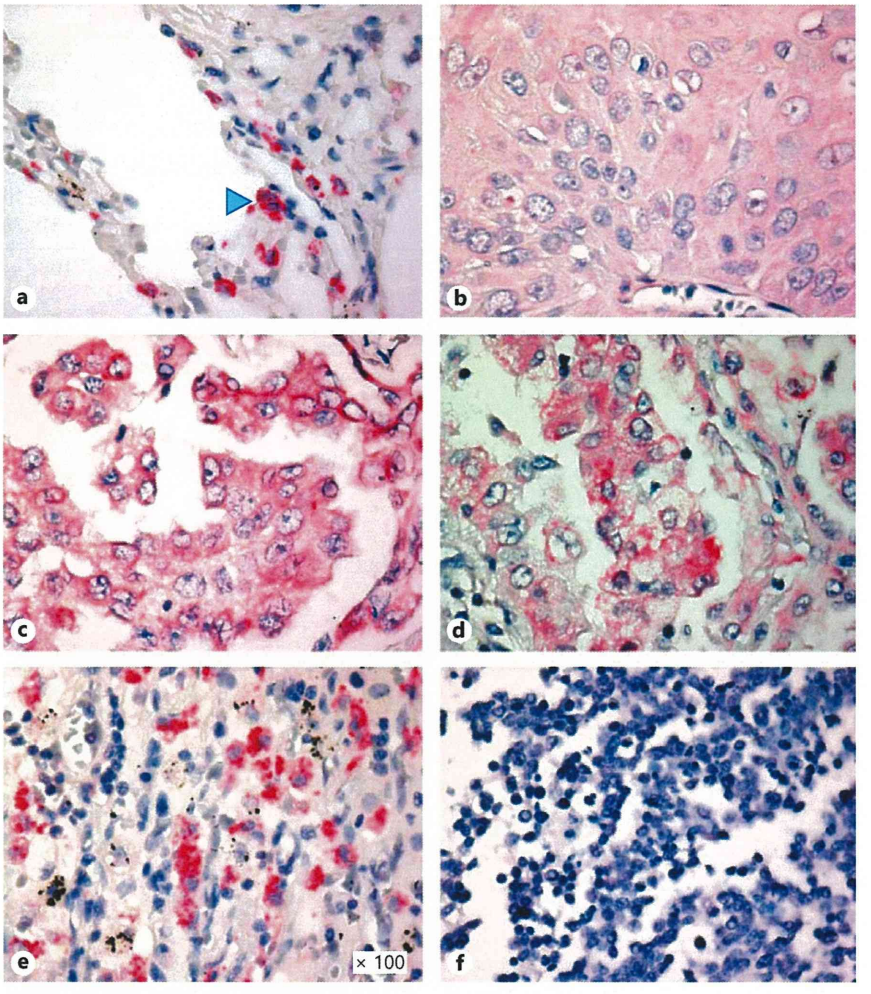

Fig. 1. Expression patterns of ABCA3 in histological subtypes of bronchial carcinoma. Tissue sections were stained by indirect immunoperoxidase reaction with a polyclonal rabbit anti-ABCA3 antibody as primary antibody, and characteristic examples for histological subtypes of bronchial carcinoma are shown. In normal adult lung tissue, ABCA3 expression was restricted to type 2 pneumocytes (**a**; arrowhead). In samples with squamous cell differentiation, the cytoplasm of the tumor cells displayed a homogeneously diffuse, faint reactivity (**b**), whereas in samples with adenocarcinoma morphology, ABCA3 expression levels were generally higher with a heterogeneous expression pattern in the tumor histology (**c**, **d**). Cells with strong ABCA3 expression with a heterogeneous pattern were found in cases of bronchoalveolar differentiation (**e**). SCLC cases did not show reactivity with the anti-ABCA3 antibody (**f**).

taxel and vinorelbine in a dose-escalating schedule and compared the susceptibility of the variants to the parental cells. Across NSCLC cell lines, we observed a significant increase in the cytostatic efficacy of cisplatin (all cell lines) and paclitaxel (A549 and NCI-H1650) in cell lines with stably silenced ABCA3 expression compared to their parental controls (fig. 3). With respect to vinorelbine, we found a tendency to increased susceptibility associated with ABCA3 suppression, albeit with lower consistency across the cell lines (fig. 3, far right column).

Discussion

We report the first data on the expression pattern and potential functional significance of ABCA3 in lung cancer, particularly in patients with predominant adenocarcinoma differentiation. These findings may have several implications for the understanding of lung cancer disease.

First, the differences in ABCA3 expression observed between NSCLC and SCLC samples add to the knowledge about the fundamental biological differences between these two disease groups. ABCA3 expression in lung cancer appears to be closely associated with adenoid differentiation, an observation recently also made in breast cancer. In mammary cancer tissue, the level of ABCA3 expression correlated with the degree of glandular differentiation, and lower levels of ABCA3 expression were associated with a more aggressive phenotype of the tumor cells [29]. This appears similar to the situation in lung cancer with low expression levels of ABCA3 in SCLC, the most aggressive variant of the disease. Clinically, SCLCs are characterized by enhanced susceptibil-

Table 2. Expression of ABCA3 in lung cancer subtypes

Characteristics		Staining intensity			
		negative/weak		intermediate/strong	
		n	%	n	%
Age, years		54.2±10.0		56.1±9.6	
Range		32–78		30–77	
Patients	Total	108	57.8	79	42.2
	Female	33	57.9	24	42.1
	Male	75	57.7	55	42.3
Histological subtype	Adenocarcinoma	22	35.5	40	64.5
	Squamous cell carcinoma	53	67.1	26	32.9
	SCLC	19	79.2	5	20.8
	Carcinoid	8	57.1	6	42.9
	Mucoepidermoid carcinoma	6	75.0	2	25.0
Grading	I	6	54.5	5	45.5
	II	41	53.2	36	46.8
	III	45	62.5	27	37.5
	Unknown	16	59.3	11	40.7
pT status	T1	19	57.6	14	42.4
	T2	67	55.8	53	44.2
	T3	19	65.5	10	34.5
	T4	3	60.0	2	40.0
pN status	N0	70	53.4	61	46.6
	N1	24	63.2	14	36.8
	N2	13	76.5	4	23.5
	N3	1	100.0	0	0.0
Pathological stage (UICC, 6th edition)	I	67	56.3	52	43.7
	II	19	51.4	18	48.6
	IIIa	18	72.0	7	28.0
	IIIb	3	60.0	2	40.0
	IV	1	100.0	0	0.0

Numbers and percentages of negative and weakly positive versus intermediate and strongly positive tumor cases are listed. Note the inverse relationship between ABCA3 positivity of high ABCA3 expression in NSCLC/adenocarcinoma tissue and low ABCA3 expression in the SCLC samples. Furthermore, major differences in gender, grading, pT/N status or pathological stage were not detected.

Table 3. Intratumoral heterogeneity of ABCA3 expression in lung cancer tissue

Histological subtype	Intermediate/strong positivity for ABCA3 cluster (positivity/tumor sample)					
	0%	≤1%	>1–≤25%	>25–≤50%	>50–≤75%	>75%
Adenocarcinoma	22 (35.5)	14 (22.6)	7 (11.3)	6 (9.7)	2 (3.2)	11 (17.7)
Squamous cell carcinoma	53 (67.1)	11 (13.9)	11 (13.9)	2 (2.5)	0	2 (2.5)
SCLC	19 (79.2)	2 (8.3)	3 (12.5)	0	0	0
Carcinoid	8 (57.1)	3 (21.4)	0	1 (7.1)	1 (7.1)	1 (7.1)
Mucoepidermoid carcinoma	6 (75.0)	1 (12.5)	1 (12.5)	0	0	0
Total	108 (57.8)	31 (16.6)	22 (11.8)	9 (4.8)	3 (1.6)	14 (7.5)

The numbers and percent of cases of intermediate and strongly positive cells per tumor sample are listed for all samples and the histological subtypes. Highest proportions of positive cells were observed in samples with adenocarcinoma differentiation.

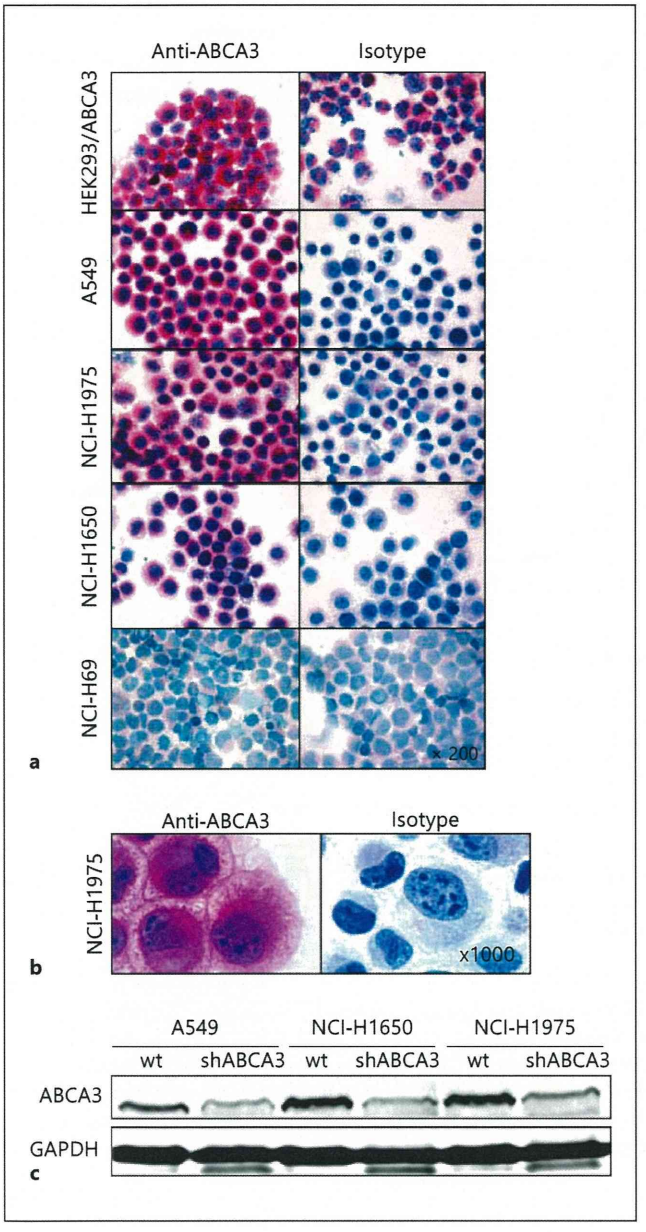

Fig. 2. Expression of ABCA3 in NSCLC and SCLC cell lines. Cell line samples were spun onto slides by cytocentrifugation and stained with anti-ABCA3 polyclonal antibody by indirect immunocytology (**a**). The expression levels in the three NSCLC cell lines A549, NCI-H1975 and NCI-H1650 were comparable to the levels achieved by enforced ectopic expression in HEK293/ABCA3 cells (**a**; upper lane). The SCLC cell line NCI-H69 showed no or very weak expression of ABCA3. As shown for NCI-H1975 at higher magnification, ABCA3 was found in a punctate pattern in the cytoplasm, with some perinuclear accumulation (**b**). ABCA3 transporter expression was also detected by Western blot in the three NSCLC cell lines (A549, NCI-H1975 and NCI-H1650), documenting significant silencing of gene expression by lentiviral shRNA transduction (**c**).

ity to cytostatic agents compared to NSCLC. In accordance with our data, the association of ABCA3 expression levels with chemotherapy resistance has also been noted in other studies. Assessing ABC transporter expression in 60 cancer cell lines (NCI-60), profiling of mRNA revealed an association of lung cancer histology and ABCA3 expression, and levels were highest in the adenocarcinoma cell lines NCI-H522, EKVX and A549 [30].

Secondly, we observed considerable intratumoral heterogeneity of ABCA3 in the primary lung cancer tissue, ranging from strong to virtually absent transporter expression in the cells of the individual cell clone (table 3). This finding is reminiscent of recent observations made on the expression of ABCA3 in leukemia and lymphoma [16, 17, 31, 32], in which transporter expression was clearly associated with a drug-resistant leukemia cell phenotype [13, 16, 17]. As for lung cancer tissue, it remains to be shown whether the strongly ABCA3-positive cells in a given tumor represent the cell fraction surviving chemotherapy, e.g. by comparing ABCA3 in tissues from primary and relapsed/refractory cases of adenocarcinoma. Different levels of heterogeneity in ABCA3 expression may reflect the wide range of response to chemotherapy. Recent observations in chronic myeloid leukemia, as well as in solid neoplasia, employing a subtractive comparative genomic hybridization-based approach to the comparison of chemotherapy-naïve and -resistant cell lines support the concept that ABCA3 expression levels increase with acquired drug resistance in cancers [33].

Third, the role of ABCA3 in the secretory function of type 2 pneumocytes, specifically its role in the formation of intracellular multilamellar bodies and consecutively extracellular multitrabecular bodies, raises the question to which extent such vesicles are secreted by cancer cells and how such vesicles might interfere with lung cancer biology and treatment. For aggressive B-cell lymphomas, we recently reported that ABCA3 is involved in tumor cell secretion of exosomes and that such tumor-derived exosomes protect cancer cells against complement-dependent cytotoxicity of therapeutic antibodies [26]. These findings were mirrored by observations in epithelial cancer cells, for which exosomal shedding of the epidermal growth factor receptor was described to allow tumor cells to evade antibody-dependent cellular cytotoxicity [34]. It is currently open to question to which extent and to which morphological subtype of extracellular vesicles the expression of ABCA3 in lung cancer cells contribute, and whether

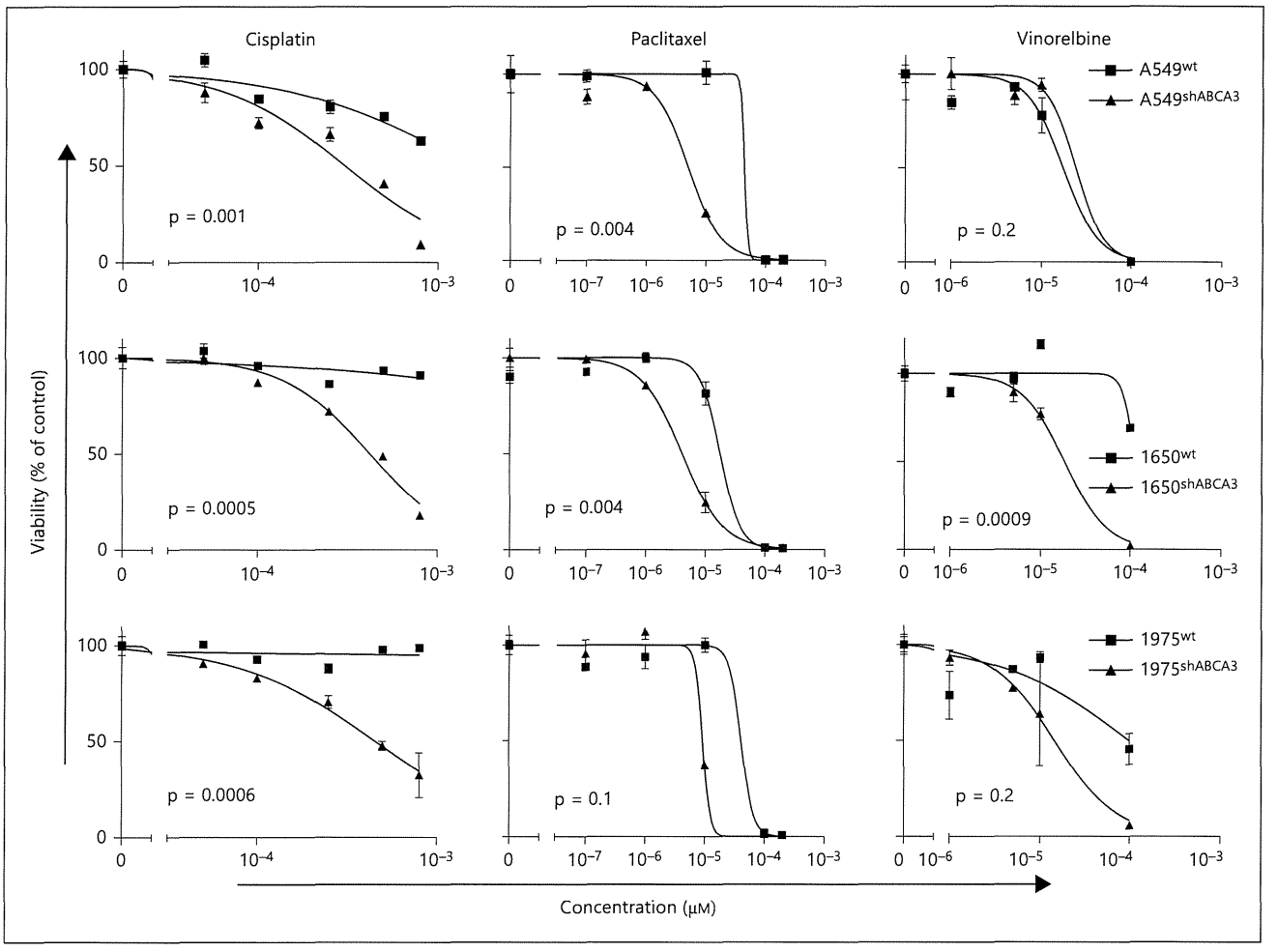

Fig. 3. Silencing of ABCA3 sensitizes lung cancer cell lines to the cytostatic effects of cisplatin and paclitaxel. Silencing of ABCA3 was achieved in the cell lines A549, NCI-H1650 and NCI-H1975 by lentiviral shABCA3 constructs and stable variant cell populations exposed to cisplatin, paclitaxel and vinorelbine for 3 h each at increasing concentrations as indicated. Viability of cells was measured by MTT test after 24 h, and values are reported as percent of untreated controls, with error bars representing standard deviations of triplicates. Differences between experimental groups were evaluated by two-way ANOVA with a Bonferroni post hoc test; p values were integrated into the graphs.

such vesicles traffic or bind chemotherapy or therapeutic antibodies.

Fourth, several further ABC transporters have been recognized to interfere with cytostatic drugs in lung cancer [35, 36]. In particular the transporter ABCB1 (MDR1, P-glycoprotein) and ABCC1 (multidrug resistance protein, MRP1) at the plasma membrane, as well as lung resistance protein at the nuclear membrane, were expressed in lung cancer cells and associated with drug resistance against classical ABC transporter substrates [37, 38]. Noteworthy, the resistance mechanisms supported by classical ABC transporter function do not alter cellular accumulation of cisplatin and do not protect cancer cells from cisplatin-mediated cytotoxicity. Thus MDR1 and MRP1 expression levels were not correlated with chemosensitivity or intracellular/intranuclear accumulation of cisplatin in several cell lines [9]. It remains to be investigated whether cisplatin is actually sequestered and exported in exocytic vesicles, as discussed above, or whether the protective effect of increased ABCA3 function is based on its effects on cellular phospholipid composition and susceptibility to proapoptotic stimuli.

Based on these data, we are now focusing on NSCLC patients treated with cisplatin-based chemotherapy in a neoadjuvant setting, and tumor samples were examined before and after systemic therapy. The aims of the following study are to detect possible changes in ABCA3 expression, particularly in chemoresistant lung cancer tumors, and to investigate the effect of different ABCA3 levels in lung cancer on the prediction of response to chemotherapy and prognosis.

Inhibitors of ABCA3 are already established and further preclinical studies in lung cancer are planned in order to elucidate potential effects in combination with systemic therapy.

Taken together, intracellular ABCA3 is differentially expressed in histological subtypes of human lung cancer and modulates susceptibility of NSCLC cell lines to cisplatin and paclitaxel in vitro. Further analysis of the subcellular mechanisms of cancer cells and the evaluation of effects from specific interference with ABCA3 function may eventually contribute to refinements in the cytostatic treatment of lung cancer.

Acknowledgments

We thank Sabrina Becker and Verena Schrader from the Department of Hematology and Oncology, Unversity Medical Center of Göttingen for their assistance in flow cytometry and viability assays. Financial support for this research was provided to T.R.O. from the research funding program of the Faculty of Medicine, Georg August University Göttingen, Germany.

Disclosure Statement

We declare that none of the authors has any financial interest related to this work.

References

1 Goeckenjan G, Sitter H, Thomas M, et al: Prevention, diagnosis, therapy, and follow-up of lung cancer: interdisciplinary guideline of the German Respiratory Society and the German Cancer Society (in German). Pneumologie 2011;65:39–59.
2 Zabel P, Hallek M: Bronchial carcinoma (in German). Internist (Berl) 2011;52:123–124.
3 Ettinger DS, Akerley W, Bepler G, et al: Non-small cell lung cancer. J Natl Compr Canc Netw 2010;8:740–801.
4 Berger W, Elbling L, Hauptmann E, et al: Expression of the multidrug resistance-associated protein (MRP) and chemoresistance of human non-small-cell lung cancer cells. Int J Cancer 1997;73:84–93.
5 Berger W, Setinek U, Hollaus P, et al: Multidrug resistance markers P-glycoprotein, multidrug resistance protein 1, and lung resistance protein in non-small cell lung cancer: prognostic implications. J Cancer Res Clin Oncol 2005;131:355–363.
6 Bessho Y, Oguri T, Ozasa H, et al: ABCC10/MRP7 is associated with vinorelbine resistance in non-small cell lung cancer. Oncol Rep 2009;21:263–268.
7 Chiou JF, Liang JA, Hsu WH, et al: Comparing the relationship of Taxol-based chemotherapy response with P-glycoprotein and lung resistance-related protein expression in non-small cell lung cancer. Lung 2003;181:267–273.
8 Chuman Y, Sumizawa T, Takebayashi Y, et al: Expression of the multidrug-resistance-associated protein (MRP) gene in human colorectal, gastric and non-small-cell lung carcinomas. Int J Cancer 1996;66:274–279.
9 Ikuta K, Takemura K, Sasaki K, et al: Expression of multidrug resistance proteins and accumulation of cisplatin in human non-small cell lung cancer cells. Biol Pharm Bull 2005;28:707–712.
10 Oguri T, Ozasa H, Uemura T, et al: MRP7/ABCC10 expression is a predictive biomarker for the resistance to paclitaxel in non-small cell lung cancer. Mol Cancer Ther 2008;7:1150–1155.
11 Yeh JJ, Hsu WH, Wang JJ, et al: Predicting chemotherapy response to paclitaxel-based therapy in advanced non-small-cell lung cancer with P-glycoprotein expression. Respiration 2003;70:32–35.
12 Young LC, Campling BG, Cole SP, et al: Multidrug resistance proteins MRP3, MRP1, and MRP2 in lung cancer: correlation of protein levels with drug response and messenger RNA levels. Clin Cancer Res 2001;7:1798–1804.
13 Hirschmann-Jax C, Foster AE, Wulf GG, et al: A distinct 'side population' of cells with high drug efflux capacity in human tumor cells. Proc Natl Acad Sci USA 2004;101:14228–14233.
14 Wulf GG, Wang RY, Kuehnle I, et al: A leukemic stem cell with intrinsic drug efflux capacity in acute myeloid leukemia. Blood 2001;98:1166–1173.
15 Wulf GG, Modlich S, Inagaki N, et al: ABC transporter ABCA3 is expressed in acute myeloid leukemia blast cells and participates in vesicular transport. Haematologica 2004;89:1395–1397.
16 Chapuy B, Panse M, Radunski U, et al: ABC transporter A3 facilitates lysosomal sequestration of imatinib and modulates susceptibility of chronic myeloid leukemia cell lines to this drug. Haematologica 2009;94:1528–1536.
17 Chapuy B, Koch R, Radunski U, et al: Intracellular ABC transporter A3 confers multidrug resistance in leukemia cells by lysosomal drug sequestration. Leukemia 2008;22:1576–1586.
18 Cheong N, Zhang H, Madesh M, et al: ABCA3 is critical for lamellar body biogenesis in vivo. J Biol Chem 2007;282:23811–23817.
19 Ban N, Matsumura Y, Sakai H, et al: ABCA3 as a lipid transporter in pulmonary surfactant biogenesis. J Biol Chem 2007;282:9628–9634.
20 Shulenin S, Nogee LM, Annilo T, et al: ABCA3 gene mutations in newborns with fatal surfactant deficiency. N Engl J Med 2004;350:1296–1303.
21 Mulugeta S, Gray JM, Notarfrancesco KL, et al: Identification of LBM180, a lamellar body limiting membrane protein of alveolar type II cells, as the ABC transporter protein ABCA3. J Biol Chem 2002;277:22147–22155.
22 Nagata K, Yamamoto A, Ban N, et al: Human ABCA3, a product of a responsible gene for abca3 for fatal surfactant deficiency in newborns, exhibits unique ATP hydrolysis activity and generates intracellular multilamellar vesicles. Biochem Biophys Res Commun 2004;324:262–268.
23 Giard DJ, Aaronson SA, Todaro GJ, et al: In vitro cultivation of human tumors: establishment of cell lines derived from a series of solid tumors. J Natl Cancer Inst 1973;51:1417–1423.
24 Sordella R, Bell DW, Haber DA, et al: Gefitinib-sensitizing EGFR mutations in lung cancer activate anti-apoptotic pathways. Science 2004;305:1163–1167.

25 Little CD, Nau MM, Carney DN, et al: Amplification and expression of the c-myc oncogene in human lung cancer cell lines. Nature 1983;306:194–196.
26 Aung T, Chapuy B, Vogel D, et al: Exosomal evasion of humoral immunotherapy in aggressive B-cell lymphoma modulated by ATP-binding cassette transporter A3. Proc Natl Acad Sci USA 2011;108:15336–15341.
27 Yamano G, Funahashi H, Kawanami O, et al: ABCA3 is a lamellar body membrane protein in human lung alveolar type II cells. FEBS Lett 2001;508:221–225.
28 Mountain CF: Revisions in the International System for Staging Lung Cancer. Chest 1997; 111:1710–1717.
29 Schimanski S, Wild PJ, Treeck O, et al: Expression of the lipid transporters ABCA3 and ABCA1 is diminished in human breast cancer tissue. Horm Metab Res 2009;42:102–109.
30 Szakács G, Annereau JP, Lababidi S, et al: Predicting drug sensitivity and resistance: profiling ABC transporter genes in cancer cells. Cancer Cell 2004;6:129–137.
31 Efferth T, Gillet JP, Sauerbrey A, et al: Expression profiling of ATP-binding cassette transporters in childhood T-cell acute lymphoblastic leukemia. Mol Cancer Ther 2006;5:1986–1994.
32 Steinbach D, Gillet JP, Sauerbrey A, et al: ABCA3 as a possible cause of drug resistance in childhood acute myeloid leukemia. Clin Cancer Res 2006;12:4357–4363.
33 Yasui K, Mihara S, Zhao C, et al: Alteration in copy numbers of genes as a mechanism for acquired drug resistance. Cancer Res 2004;64: 1403–1410.
34 Battke C, Ruiss R, Welsch U, et al: Tumour exosomes inhibit binding of tumour-reactive antibodies to tumour cells and reduce ADCC. Cancer Immunol Immunother 2011;60:639–648.
35 Stavrovskaya AA, Stromskaya TP: Transport proteins of the ABC family and multidrug resistance of tumor cells. Biochemistry (Mosc) 2008;73:592–604.
36 Munoz M, Henderson M, Haber M, et al: Role of the MRP1/ABCC1 multidrug transporter protein in cancer. IUBMB Life 2007;59:752–757.
37 Cole SP, Bhardwaj G, Gerlach JH, et al: Overexpression of a transporter gene in a multidrug-resistant human lung cancer cell line. Science 1992;258:1650–1654.
38 Cole SP, Deeley RG: Multidrug resistance-associated protein: sequence correction. Science 1993;260:879.

ORIGINAL ARTICLE

Sorting nexin 19 regulates the number of dense core vesicles in pancreatic β-cells

Shin-ichi Harashima[1]*, Takahiko Horiuchi[2], Yu Wang[1], Abner Louis Notkins[3], Yutaka Seino[1], Nobuya Inagaki[1]

ABSTRACT

Aims/Introduction: Insulinoma-associated protein 2 (IA-2) regulates insulin secretion and the number of dense core vesicles (DCV). However, the mechanism of regulation of DCV number by IA-2 is unknown. We examined the effect of sorting nexin 19 (SNX19), an IA-2 interacting protein, on insulin secretion and the number of dense core vesicles (DCV).

Materials and Methods: Stable SNX19 knockdown (SNX19KD) MIN6, a mouse pancreatic β-cell line, and stable SNX19-reintroduced SNX19KD MIN6 were established. Quantification of DCV, and lysosomes was carried out using electron micrographs. The half-life of DCV was detected by pulse-chase experiment.

Results: Insulin secretion and content were decreased in stable SNX19KD MIN6 cells compared with those in control MIN6 cells. Electron micrographs showed that DCV number in SNX19KD cells was decreased by approximately 75% and that DCV size was decreased by approximately 40% compared with those in control cells, respectively. Furthermore, when SNX19 was reintroduced in SNX19KD cells, insulin content, insulin secretion and DCV number were increased. The half-life of DCV was decreased in SNX19KD cells, but was increased in SNX19KD cells in which SNX19 was reintroduced. The number of lysosomes and the activity of lysosome enzyme cathepsin D were increased by approximately threefold in SNX19KD cells compared with those in control cells. In contrast, they were decreased to approximately half to one-third in SNX19-reintroduced SNX19KD cells.

Conclusions: SNX19 regulates the number of DCV and insulin content by stabilizing DCV in β-cells. (J Diabetes Invest, doi: 10.1111/j.2040-1124.2011.00138.x, 2012)

KEY WORDS: Sorting nexin 19, Insulinoma-associated protein 2, Dense core vesicles

INTRODUCTION

The sorting nexins (SNX) belong to a large family involved in protein sorting and intracellular trafficking[1,2]. SNX19 is a 992 amino acid member of this family that has a phox (PX) domain (a binding motif to phosphatidylinositol) at the COOH-terminus and a PX-associated (PXA) domain at the NH2-terminus[3,4]. The function of SNX19 is not known, but it binds to the dense core vesicle (DCV) transmembrane protein insulinoma-associated protein 2 (IA-2)[5].

IA-2 is a major autoantigen in type 1 diabetes[6,7], and autoantibodies to it are found in 70–80% of newly diagnosed patients. These autoantibodies appear years before the onset of clinical disease, and individuals with autoantibodies to both IA-2 and GAD65 have approximately a 50% risk of developing type 1 diabetes within 5 years. Based on sequence, IA-2 is a member of the protein tyrosine phosphate (PTP) family, but because of two amino acid substitutions in the PTP domain, it is enzymatically inactive with conventional PTP substrates[8]. IA-2 is present in neuroendocrine cells throughout the body and knockout of IA-2 in mice results in impaired secretion of hormones and neurotransmitters, and a variety of phenotypes characterized by impaired insulin secretion, glucose intolerance[9,10], female infertility[11], abnormalities in learning and behavior[12], and loss of circadian rhythm[13]. Overexpression of IA-2 in MIN6 cells and rat pheochromocytoma cell line PC12 cells increased insulin secretion[14] and dopamine release[15], respectively.

Because SNX19 binds to IA-2, the present experiments were initiated to study the effects of knockdown and reconstitution of SNX19 in MIN6 cells on the biology and physiology of DCV, including their half-life, and number and the cellular content and secretion of insulin. We show here that SNX19 regulates the DCV number and insulin content by modulating the half-life of DCV in pancreatic β-cells.

MATERIALS AND METHODS

Reagents

pCMV-Tag3 mammalian expression vectors with G418 resistance gene were purchased from Agilent technologies (Santa Clara, CA, USA), pSilencer3.1-CMV hygro mammalian siRNA expression vector from Applied Biosystem (Austin, TX, USA), Effectene transfection reagent from Qiagen (Santa Clarita, CA, USA), mouse IA-2 antibody from LAD (Berlin, Germany), mouse anti-α-tubulin antibody from Sigma (St. Louis, MO,

[1]Department of Diabetes and Clinical Nutrition, Graduate School of Medicine, Kyoto University, Kyoto, [2]Department of Medicine and Biosystemic Science, Graduate School of Medical Sciences, Kyushu University, Fukuoka, Japan, and [3]Experimental Medicine Section, Oral Infection and Immunity Branch, National Institute of Dental and Craniofacial Research (NIDCR), National Institutes of Health (NIH), Bethesda, MD, USA
*Corresponding author. Shin-ichi Harashima Tel.: +81-75-751-3560
Fax: +81-75-771-6601 E-mail address: harasima@metab.kuhp.kyoto-u.ac.jp
Received 22 March 2011; revised 12 April 2011; accepted 2 May 2011

USA), anti-SNX19 antibody from Santa Cruz biotechnology (Santa Cruz, CA, USA) and mouse insulin ELISA kit from Shibayagi (Shibukawa, Japan).

Plasmids

Two SNX19 siRNA were synthesized by Takara (Otsu, Japan); the sequences were 5′-AATTGCACCTGGAACGATTCA-3′ and 5′-AAAGGCAGCTGGAACAGGAGA-3′, and were inserted into pSilencer 3.1-CMV hygro vector. Primers for complementary SNX19 were synthesized by Takara. The forward and reverse primer sequences for SNX19 were 5′-CCGCTCGAGATGAAGACAGAAACAGTG-3′ and 5′-CCGCTCGAGCTAAGAGGAGACACCCAT-3′. SNX19 polymerase chain reaction (PCR) product was inserted into pCMV-Tag3 at *Xho*I sites. All plasmids were sequenced and no mutations were found.

Establishment of Stable Cell Lines

MIN6 cells were maintained in Dulbecco's modified Eagle's medium (DMEM) containing 25 mmol/L D-glucose (high glucose), supplemented with 15% heat-inactivated fetal bovine serum, 100 U/mL penicillin and 100 μg/mL streptomycin at 37°C in 95% air and 5% CO_2. SNX19 siRNA inserted into pSilence3.1-CMV hygro vector were introduced into MIN6 cells with Effectene transfection reagent, and stably transfected cells were selected by 200 μg/mL of hygromycin and by limiting dilution. Full length IA-2 and full length SNX19 were inserted into pCMV-Tag3 vectors and introduced into SNX19 knockdown MIN6 cells using Effectene transfection reagent, and stably transfected cells were selected by 300 μg/mL of G418 and 200 μg/mL of hygromycin, and by limiting dilution. SNX19 and IA-2 expression were confirmed by western blot.

Western Blot

Cells were washed twice with PBS, detached from plates with trypsin-EDTA, collected, washed two more times with PBS and then sonicated in lysis buffer. Equivalent amounts of protein were resolved by sodium dodecyl sulfate–polyacrylamide gel electrophoresis on 4–12% acrylamide gels (Invitrogen, Carlsbad, CA, USA) and transferred to polyvinylidene fluoride membranes (Invitrogen), followed by immunoblotting with antibodies to detect respective proteins.

Cell Proliferation Assay

A total of 1.0×10^4 cells/mL were seeded into a 96-well culture late and incubated for 10 days in 25 mmol/L glucose DMEM media. Cell proliferation was measured at indicated times by a bromodeoxyuridine (BrdU) cell proliferation assay kit (Calbilchem, Damstadt, Germany) as previously reported[16].

Insulin Secretion Test

MIN6 cells were seeded in 96-well culture plates at a density of 3.0×10^4 cells per well and cultured for 3 days. The attached cells were washed twice with 3 mmol/L glucose Krebs–Ringer bicarbonate HEPES (KRBH) buffer (124 mmol/L NaCl, 5.6 mmol/L KCl, 2.5 mmol/L $CaCl_2$ and 20 mmol/L HEPES at pH 7.4). The cells were then incubated at 37°C for 60 min in KRBH buffer, washed and incubated again for 60 min in KRBH at 3 mmol/L glucose. Supernatant was collected and insulin release measured by ELISA kit (Shibayagi). The cells then were incubated at 25 mmol/L glucose in KRBH for 60 min and the amount of insulin released measured again.

Insulin Content

Cells were seeded in 24-well culture plates at a density of 1.0×10^5 cells per well and cultured for 3 days at 25 mmol/L glucose. Media then were removed and replaced again with 25 mmol/L glucose. The cells were incubated for 16 h and the insulin content was determined by ELISA.

Electron Microscopy

Cells were cultured in 25 mmol/L glucose for 3 days. The culture media then were replaced with 25 mmol/L glucose containing fresh DMEM media for 16 h. Cells were washed with PBS three times and fixed with 2.5% glutaraldehyde in 0.1 mol/L phosphate buffer, pH 7.4, and used for electron microscopy study.

Quantification of DCV and Lysosomes Per Cytoplasmic Area

Quantification of DCV was carried out as previously reported[14]. Briefly, 15 cells were selected at random and the images were taken at 8 k magnification. The number of DCV/cytoplasmic area or lysosome/cytoplasmic area was quantified by two operators blind to their status using national Institutes of Health images. Approximately 20 cytoplasmic areas taken by electron microscopy were estimated.

Half-life of DCV

Insulin half-life was determined as previously described[14]. Cells were seeded in 6-well culture plates and incubated for 2 days in 25 mmol/L glucose to obtain a steady state. The cells were then washed with KRBH buffer and incubated in 25 mmol/L glucose luecine-free media with [^{3}H]leucine (Amersham Biosciences, Piscataway, NJ, USA) for 24 h. The media then was changed to 3 mmol/L low glucose without [^{3}H]leucine for a 48 h chase. The cells and supernatant were collected at different times and the cells were lysed by repeated freezing and thawing. The cell lysates and supernatants were incubated at 4°C for 2 h in the presence of anti-insulin or anti-proinsulin antibodies. Antibody-antigen complexes then were precipitated by adding 5 mg of protein A-Sepharose in 100 μL of glycine/BSA/NP-40 buffer. After mixing at 4°C for 2 h, the immunoreactive material bound to the protein A-Sepharose was separated from unbound material in the supernatant by centrifugation (8000 *g*, 30 s). After washing the precipitates twice with 250 μL of glycine/BSA/NP-40, the precipitants were suspended in 250 μL of 1 mol/L acetic acid and 2.5 mg/mL of BSA. The suspended precipitates were added to liquid scintillation vials, the activity ratios measured and the insulin half-life determined. Incorporation of

[^{3}H]leucine into total protein under high glucose over 24 h was determined by precipitation with trichloroacetic acid (TCA). The data is expressed as the ratio of radiolabeled (pro)insulin/TCA precipitated protein.

Cathepsin D Activity

To measure cathepsin D activity, 1.0×10^4 cells were thoroughly washed in glucose-free Hank's solution and dissolved by sonication in 200 mL acetate-EDTA buffer (1.1 mmol/L

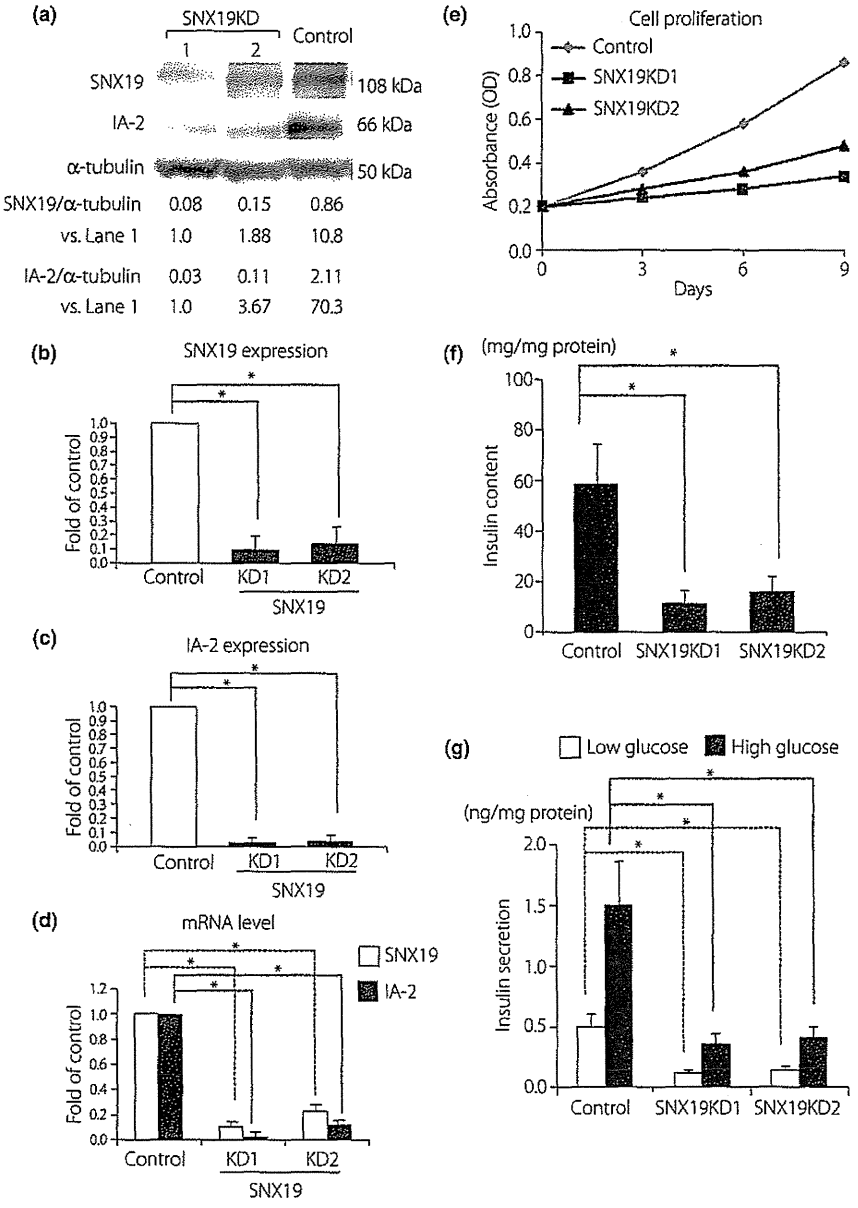

Figure 1 | Decrease in sorting nexin 19 (SNX19) expression slowed cell proliferation and reduced insulin content and insulin secretion. (a) Establishment of SNX19 knockdown MIN6 cells. Western blot analysis of SNX19 and insulinoma-associated protein 2 (IA-2) expression in sorting nexin 19 knockdown (SNX19KD) and control MIN6 cells. (b) Relative ratio of SNX19 expression in SNX19KD MIN6 cells compared with that in control MIN6 cells. (c) Relative ratio of IA-2 expression in SNX19KD MIN6 cells compared with that in control MIN6 cells. (d) Relative ratio of mRNA level of SNX19 or IA-2 quantified by real time polymerase chain reaction in SNX19KD MIN6 cells compared with that in control MIN6 cells. (e) Cell proliferation measured by a bromodexyuridine cell proliferation assay in control, SNX19KD MIN6 cells. (f) Insulin content in control and SNX19KD MIN6 cells. (g) Low (3 mmol/L) and high (25 mmol/L) glucose-stimulated insulin secretion in control and SNX19KD MIN6 cells. Images are representative of three independent experiments. Data are means ± SE of four independent experiments. *$P < 0.01$.

EDTA, 5 mmol/L acetate, pH 5.0). Aliquots were used to measure lysosomal activity determined by cathepsin D activity kit (Sigma).

Statistical Analysis

All data are expressed as mean ± standard error. Student's *t*-test was used to determine statistical significance.

RESULTS

Knockdown of SNX19 Decreases Insulin Content and Insulin Secretion in MIN6 cells

We established two permanent SNX19 knockdown (SNX19KD) MIN6 cell lines (SNX19KD1 and SN19KD2). Western blot showed that SNX19 expression was decreased to approximately one-tenth and one-fifth in SNX19KD1 and SNX19KD2 MIN6 cells, respectively, compared with that in scrambled siRNA-expressing MIN6 cells (control; Figure 1a,b). IA-2 expression was decreased to less than one-thirtieth in SNX19KD1 and SNX19KD2 MIN6 cells compared with that in control MIN6 cells (Figure 1a,c). Quantitative real-time PCR showed that messenger RNA level of SNX19 was decreased by approximately one-tenth and one-fifth in SNX19KD1 and SNX19KD2 MIN6 cells, respectively (Figure 1d). Messenger RNA level of IA-2 also was decreased by one-thirtieth and one-tenth in SNX19KD1 and SNX19KD2 MIN6 cells, respectively, as observed in western blot (Figure 1d). Cell proliferation of the SNX19KD cells were decreased by approximately one-third to one-quarter compared with that of control cells (Figure 1e). As a reduction in IA-2 expression and cell proliferation in pancreatic β-cells is known to decrease insulin content and secretion[9,14], we examined insulin content and glucose-stimulated insulin secretion in SNX19KD MIN6 cells. Insulin content was

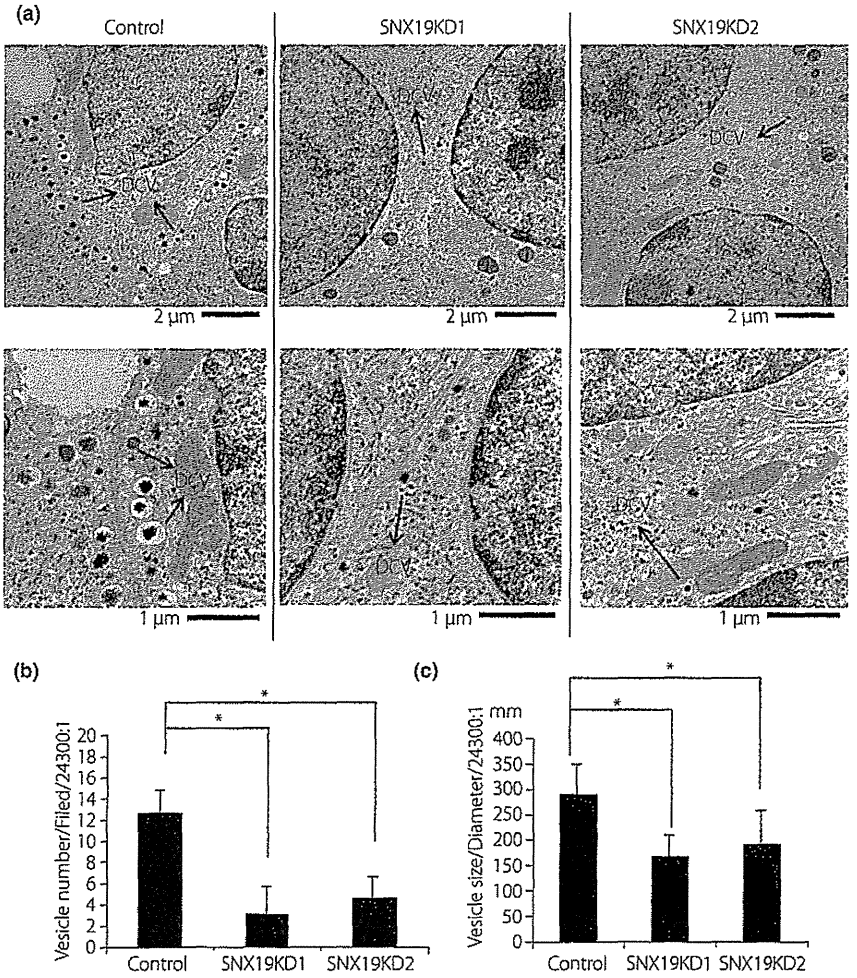

Figure 2 | Knockdown of sorting nexin 19 (SNX19) decreased the number of dense core vesicles (DCV). (a) Representative electron micrographs of 15 images in control, sorting nexin 19 knockdown (SNX19KD)1 and SNX19KD2 MIN6 cells. Black arrows indicate DCV. (b) Average number of DCV in control, SNX19KD1 and SNX19KD2 MIN6 cells. (c) Average size of DCV in control, SNX19KD1 and SXN19KD2 MIN6 cells. Data are means ± SE of four independent experiments. *$P < 0.01$.

decreased to one-seventh and one-quarter in SNX19KD1 and SNX19KD2 MIN6 cells, respectively, compared with that in control MIN6 cells (Figure 1f). The amounts of constitutive and glucose-stimulated insulin secretion also were decreased to approximately one-quarter and one-third in SNX19KD1 and SNX19KD2 cells, respectively, compared with that in control MIN6 cells (Figure 1g). These results suggest that SNX19 regulates insulin content and insulin secretion with a decrease in IA-2 expression.

Knockdown of SNX19 Decreases the Number and the Size of DCV in MIN6 Cells

We then examined the number of DCV in SNX19KD MIN6 cells. Electron micrographs showed that the number of DCV

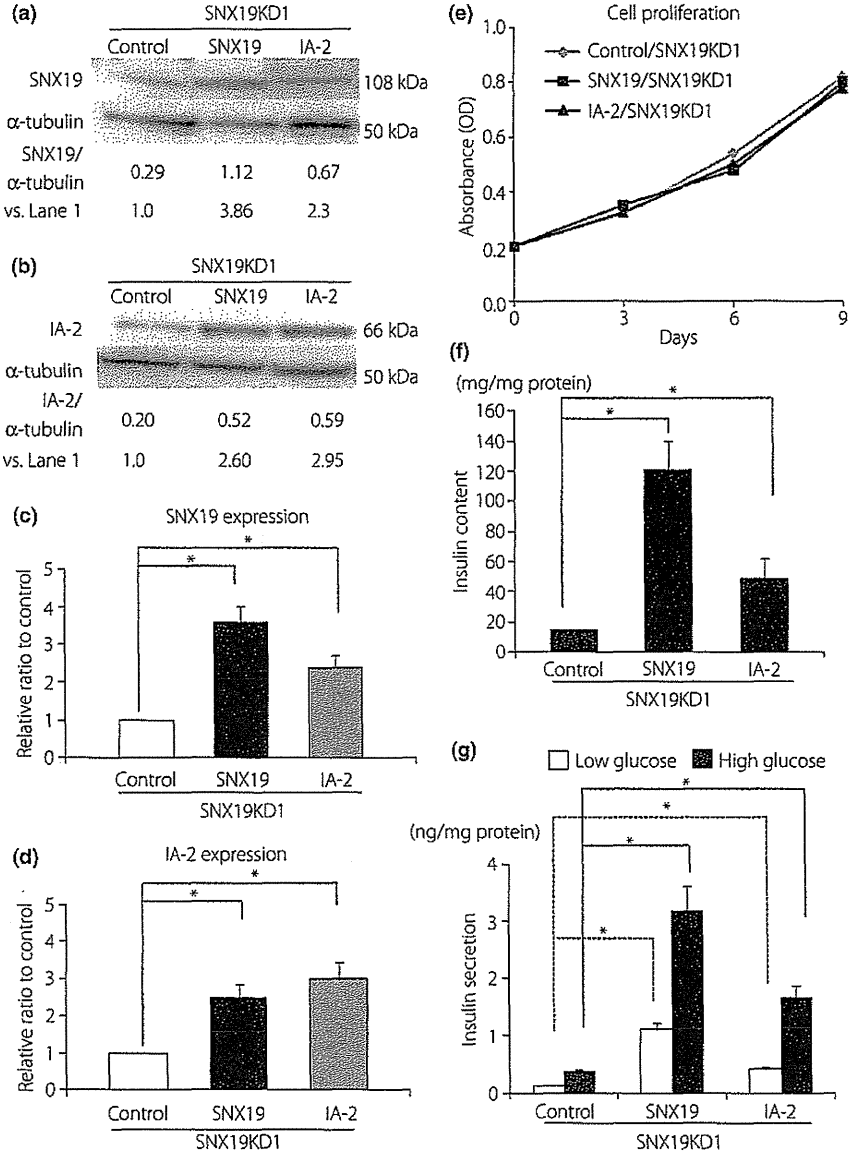

Figure 3 | Reintroduction of sorting nexin 19 (SNX19) or insulinoma-associated protein 2 (IA-2) in sorting nexin 19 knockdown (SNX19KD) MIN6 cells restored cell proliferation rate, insulin content and insulin secretion. (a) Western blot analysis of SNX19 expression in control, SNX19/ and IA-2/SNX19KD1 MIN6 cells. (b) Western blot analysis of IA-2 expression in control, SNX19/ and IA-2/SNX19KD1 MIN6 cells. (c) Relative ratio of SNX19 expression in SNX19/ and IA-2/SNX19KD1 MIN6 cells compared with that in control/SNX19KD1 MIN6 cells. (d) Relative ratio of IA-2 expression in SNX19/ and IA-2/SNX19KD1 MIN6 cells compared with that in control/SNX19KD1 MIN6 cells. (e) Cell proliferation measured by a bromodexyuridine cell proliferation assay in control/, SNX19/ and IA-2/SNX19KD1 MIN6 cells. (f) Insulin content in control/, SNX19/ and IA-2/SNX19KD1 MIN6 cells. (g) Low (3 mmol/L) and high (25 mmol/L) glucose-stimulated insulin secretion in control/, SNX19/ and IA-2/SNX19KD1 MIN6 cells. Images are representative of three independent experiments. Data are means ± SE of four independent experiments. *$P < 0.01$.

was dramatically decreased in SNX19KD1 and SNX19KD2 MIN6 cells compared with that in control cells (Figure 2a). In addition, the size of DCV was smaller in SNX19KD1 and SNX19KD2 MIN6 cells compared with that in control cells (Figure 2a). The average number of DCV was decreased to approximately one-sixth and one-quarter in SNX19KD1 and SNX19KD2 MIN6 cells, respectively, compared with that in control cells (Figure 2b). The size of DCV in SNX19KD1 and SNX19KD2 MIN6 cell lines were also decreased by approximately 40 and 35%, respectively, compared with that in control cells (Figure 2c).

Reintroduction of SNX19 and IA-2 in SNX19KD MIN6 Cells Restores Insulin Content and Insulin Secretion

To confirm the effect of SNX19 on the number of DCV, we used established permanent human SNX19-reintroduced SNX19KD1 (SNX19/SNX19KD1) MIN6 cells and human IA-2-reintroduced SNX19KD1 (IA-2/SNX19D1) MIN6 cells. Western blot analysis showed that SNX19 expression was increased by fourfold in SNX19/SNX19KD1 cells and by approximately twofold in IA-2/SNX19KD1 cells, respectively, compared with that in control vector-transfected SNX19KD1 cells (control/SNX19KD1; Figure 3a,c). In addition, IA-2 expression was

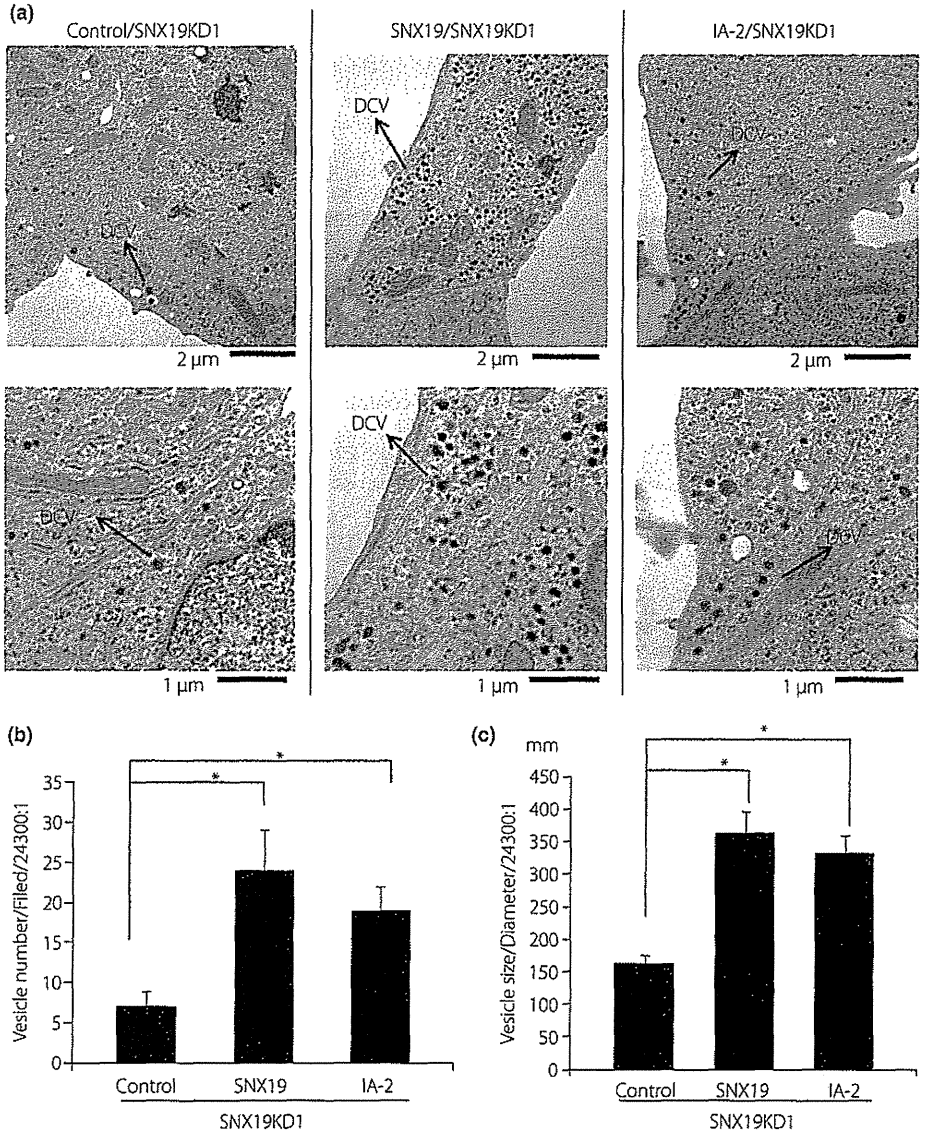

Figure 4 | Reintroduction of sorting nexin 19 (SNX19) or insulinoma-associated protein 2 (IA-2) restored the number of dense core vesicles (DCV). (a) Representative electron micrographs of 15 images in control, SNX19/ sorting nexin 19 knockdown (SNX19KD)1 and IA-2/SNX19KD1 MIN6 cells. Black arrows indicate DCV. (b) Average number of DCV in control, SNX19/SNX19KD1 and IA-2/SNX19KD1 MIN6 cells. (c) Average size of DCV in control, SNX19/SNX19KD1 and IA-2/SXN19KD1 MIN6 cells. Data are means ± SE of four independent experiments. *$P < 0.01$.

increased by approximately 2.5-fold in SNX19/SNX19KD1 MIN6 cells and approximately threefold in IA-2/SNX19KD1 MIN6 cells, respectively (Figure 3b,d). Cell proliferation of SNX19/SNX19KD1 and IA-2/SNX19KD1 MIN6 cells were almost the same as that of control/SNX19KD1 MIN6 cells (Figure 3e). Accordingly, insulin content was increased by approximately sevenfold and threefold in SNX19/SNX19KD1 and IA-2/SNX19KD1 cells, respectively, compared with that in control/SNX19KD1 cells (Figure 3f). Constitutive and glucose-stimulated insulin secretion also were increased by approximately sixfold and threefold in SNX19/SNX19KD1 and IA-2/SNX19KD1 cells, respectively, compared with those in control/SNX19KD1 cells (Figure 3g).

Reintroduction of SNX19 and IA-2 Increases the Number and the Size of DCV in SNX19KD MIN6 Cells

Electron micrographs showed that the number of DCV was increased in both SNX19/SNX19KD1 and IA-2/SNX19KD1 MIN6 cells compared with that in control/SNX19KD1 cells (Figure 4a). The number of DCV was increased by approximately fourfold in SNX19/SNX19KD1 cells and approximately threefold in IA-2/SNX19KD1 cells, respectively, compared with that in control/SNX19KD1 cells (Figure 4b). The size of DCV was increased by approximately twofold in both SNX19/SNX19KD1 and IA-2/SNX19KD1 cells compared with that in control/SNX19KD1 MIN6 cells (Figure 4c).

SNX19 Affects the Half-life of DCV

To investigate the involvement of SNX19 in DCV stability, we measured the half-life of DCV in SNX19KD1 and SNX19/SNX19KD1 cells. A pulse-chase experiment showed that the half-life of DCV in SNX19KD1 cells was 11.6 h, approximately half of that in control cells (Figure 5a). In contrast, the half-life of DCV in SNX19/SNX19KD1 was 30.4 h, approximately threefold of that in control/SNX19KD1 cells (Figure 5b). To ascertain that the decreased half-life of DCV in SNX19KD1 cells was not the result of a decrease in biosynthesis of proinsulin/insulin, cells were pulsed with [^{3}H]leucine, and newly synthesized proinsulin/insulin was measured. At the end of a 24-h pulse, the amount of proinsulin/insulin in SNX19KD1 cells was almost equal to or slightly lower than that in control cells (Figure 5a). Similarly, the amount of newly synthesized proinsulin/insulin in SNX19/SNX19KD1 cells was almost equal to or slightly greater than that in control/SNX19KD1 cells (Figure 5b). These results show that SNX19 stabilizes DCV.

SNX19 Knockdown Increases the Activity of Lysosomes

The finding that SNX19 affected the half-life of DCV suggested that the reduction of DCV number in the SNX19KD cells might be the result of accelerated DCV degradation. The number of lysosomes in SNX19KD1 cells was increased by approximately fourfold compared with that in control MIN6 cells (Figure 6a,b). In contrast, the number of lysosomes in SNX19/SNX19KD1

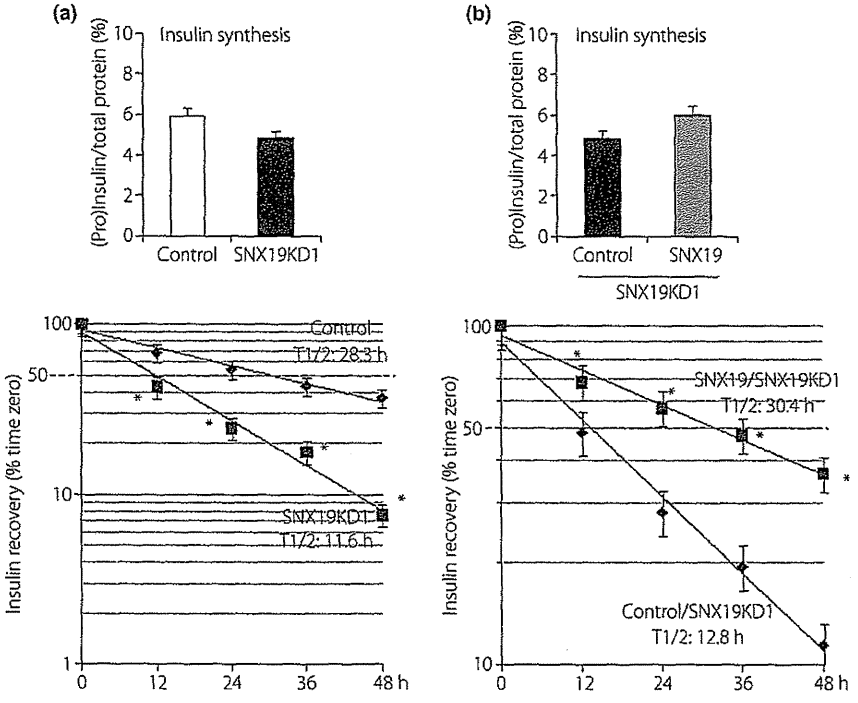

Figure 5 | Sorting nexin 19 (SNX19) affected the half-life of dense core vesicles (DCV). (a) Half-life of DCV and insulin and proinsulin biosynthesis in control and sorting nexin 19 knockdown (SNX19KD)1 MIN6 cells; (b) in control/ and SNX19/SNX19KD1 MIN6 cells. Data are means ± SE of four independent experiments. *$P < 0.01$.

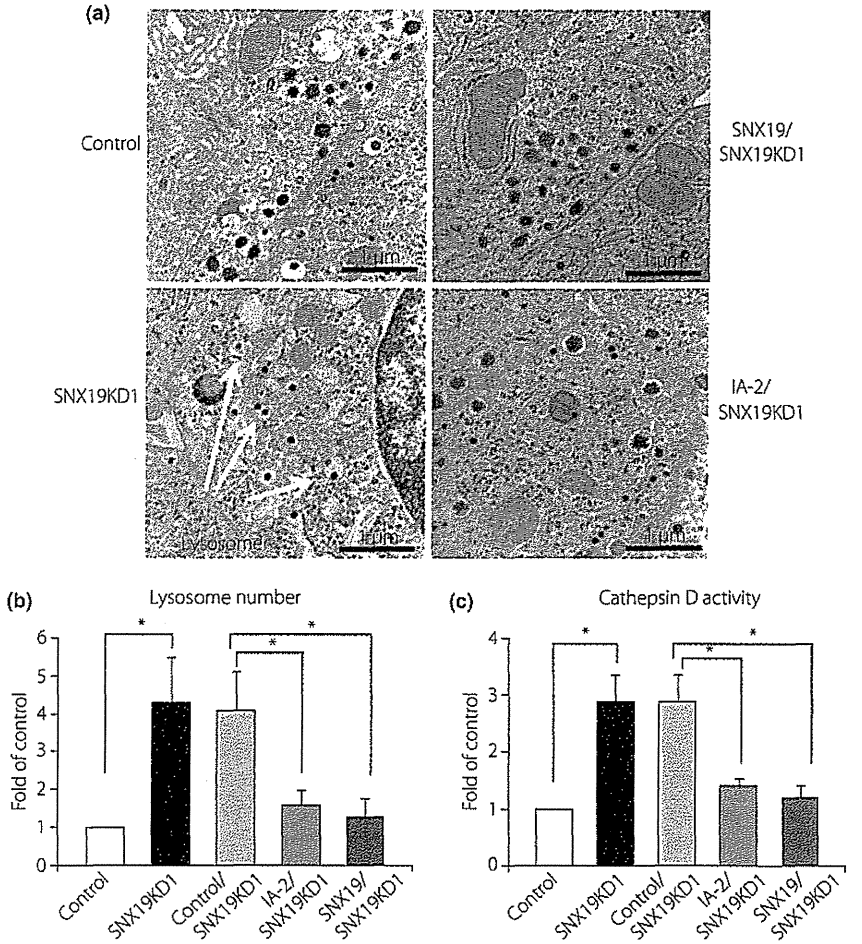

Figure 6 | Decreased expression of sorting nexin 19 (SNX19) increased activity of lysosomes and autophagy. (a) Representative electron micrographs of 15 images in control, sorting nexin 19 knockdown (SNX19KD)1, IA-2/SNX19KD1 and SNX19/SNX19KD1 MIN6 cells. White arrows indicate lysosomes. (b) Average lysosome number per image of 20 images. (c) Cathepsin D activity. Data are means ± SE of four independent experiments. *$P < 0.01$.

and IA-2/SNX19KD1 cells was almost equal to that in control cells and less than one-third of that in control/SNX19KD1 cells (Figure 6a,b). Activity of lysosome enzyme cathepsin D also was increased by approximately threefold in SNX19KD1 cells compared with that in control cells (Figure 6c), whereas activity of cathepsin D in IA-2/ and SNX19/SNX19KD1 cells was decreased to approximately half of that in control/SNX19KD1 cells (Figure 6c).

DISCUSSION

The experiments reported in the present study show that knockdown of SNX19 decreases the number of DCV in MIN6 cells, and also decreases the cellular content and secretion of insulin. Conversely, reintroduction of SNX19 increases the number of DCV in MIN6 cells, and increases the cellular content and secretion of insulin. Thus, SNX19 expression is regulated at the transcriptional level and affects the half-life of DCV, insulin content and secretion. The half-life of DCV in SNX19KD cells was 11.6 h as compared with 28.3 h in control cells and reintroduction of SNX19 increased the half-life of DCV in SNX19KD cells from 12.8 to 30.4 h. The most likely explanation for these findings is that the reduced half-life of the DCV is responsible for their reduced number, which directly underlies the decrease in insulin content and secretion.

Of particular interest, earlier experiments showed that overexpression of IA-2 in MIN6 cells significantly increased the half-life of the DCV, as well as the content and secretion of insulin[14]. Indeed, a very recent experiment found that IA-2 or IA-2β single knockout and IA-2/IA-2β double knockout mice showed a significant decrease in the number of DCV and the content and secretion of insulin (Cai T and Notkins AL, unpublished data, 2011).

IA-2 and IA-2β are transmembrane proteins on the DCV and it is thought that knockout (Cai T and Notkins AL,

unpublished data, 2011) or overexpression of these proteins[14] can decrease or increase, respectively, the stability of the DCV and, in turn, their half-life. Changes in the number of DCV transmembrane proteins can readily affect the stability of these vesicles. SNX19, however, is not a transmembrane protein, but, as determined by the yeast two hybrid system, binds to the cytoplasmic region of IA-2 encompassing amino acids 744–979[5]. Furthermore, SNX19 alone or the IA-2/SNX19 complex binds to several phosphatidylinositols (ptdlins), most strongly to Ptdins(3)P, Ptdlins(4)P and Ptdlins(5)P[16]. In contrast, IA-2 does not bind to the ptdlins. Ptdins(3)P is involved in the recruitment of many different proteins that are important for protein trafficking to membrane[17–19]. PtdIns(4)P is located in the membrane of the Golgi apparatus, and binds to the ADP ribosylation factor (ARF) GTP-binding protein and to four-phosphate-adaptor protein 1 and 2 (FAPP1 and FAPP2) and effector proteins[18,20]. This complex of molecules recruits proteins to the membrane. The function of PtdIns(5)P remains unknown, but it might act in membrane trafficking from late endosomes to the plasma membrane[20,21]. We suggest that binding of the IA-2/SNX19 complex to the ptdlins might be responsible for sorting, trafficking and stabilization of the DVC. In SNX19KD MIN6 cells, lysosomal activities are increased, restored by reintroduction of SNX19 or IA-2. Knockdown of SNX19 decreases IA-2 expression; reintroduction of SNX19 increases IA-2 expression in MIN6 cells. Thus, SNX19 regulates IA-2 expression to allow a complex of SXN19 and IA-2 to stabilize the DCV. Decreased expression of SNX19 reduces IA-2 expression and destabilizes DCV, resulting in increasing lysosomal activities and decreasing DCV half-life. Although the mechanism is not known precisely, based on our findings, the binding of SNX19 to IA-2 might be directly involved in the stabilization of DCV by exposing or protecting IA-2 from degradation or by affecting trafficking or recycling of the DCV through the endosome pathway.

SNX19 also was found to affect cell proliferation. Knockdown of SNX19 inhibited cell proliferation, which was restored by reintroduction of SNX19. We previously reported that overexpression of IA-2 and/or SNX19 induced apoptosis and inhibited cell proliferation together with a decrease in Akt/PKB phosphorylation under high glucose conditions[16]. In contrast, knockdown of IA-2 and/or SNX19 did not induce apoptosis in β-cells (data not shown). However, cell proliferation was inhibited in SNX19 knockdown MIN6 cells with a decrease in insulin content and insulin secretion. On the other hand, reintroduction of SNX19 or IA-2 restored cell proliferation in SNX19KD MIN6 cells with an increase in insulin content and insulin secretion. A possible explanation is that a decrease in insulin secretion, which is important for cell growth in pancreatic β-cells, contributes to inhibition of cell proliferation in SNX19KD MIN6 cells.

In conclusion, the present study shows the importance of SNX19 in DCV physiology. Recent studies have shown that SNX19 can bind not only to IA-2, but also to IA-2β (S.-I. Harashima, unpublished data, 2011). As there are nearly 30 different members of the SNX family, it is an intriguing group of proteins for further study.

ACKNOWLEDGEMENTS

This study was supported by Scientific Research Grants from the Ministry of Education, Culture, Sports, Science, and Technology, Japan, and from the Ministry of Health, Labor, and Welfare, Japan, and also by Kyoto University Global COE Program 'Center for Frontier Medicine'.

REFERENCES

1. Worby CA, Dixon JE. Sorting out the cellular functions of sorting nexins. *Nat Rev Mol Cell Biol* 2002; 3: 919–931.
2. Cullen PJ. Endosomal sorting and signaling: an emerging role for sorting nexins. *Nat Rev Mol Cell Biol* 2009; 9: 574–582.
3. Xu Y, Seet LF, Hanson B, *et al.* The phox homology (PX) domain, a new player in phosphoinositide signaling. *Biochem J* 2001; 360: 513–530.
4. Seet LF, Hong W. The Phox (PX) domain proteins and membrane traffic. *Biochim Biophys Acta* 2006; 1761: 878–896.
5. Hu YF, Zhang HL, Cai T, *et al.* The IA-2 interactome. *Diabetologia* 2005; 48: 2576–2581.
6. Lan MS, Lu J, Goto Y, *et al.* Molecular cloning and identification of a receptor-type protein tyrosine phosphatase, IA-2, from human insulinoma. *DNA Cell Biol* 1994; 13: 505–514.
7. Notkins AL, Lernmark A. Autoimmune type 1 diabetes: resolved and unresolved issues. *J Clin Invest* 2001; 108: 1247–1252.
8. Magistrelli G, Toma S, Isacchi A. Substitution of two variant residues in the protein tyrosine phosphatase-like PTP35/IA-2 sequence reconstitutes catalytic activity. *Biochem Biophys Res Commun* 1996; 227: 581–588.
9. Saeki K, Zhu M, Kubosaki A, *et al.* Target disruption of the protein tyrosine phosphase-like molecule IA-2 results in alterations in glucose tolerance tests and insulin secretion. *Diabetes* 2002; 51: 1284–1850.
10. Kubosaki A, Nakamura S, Notkins AL. Dense core vesicle protein IA-2 and IA-2{beta}: metabolic alterations in double knockout mice. *Diabetes* 2005; 54: s46–s51.
11. Kubosaki A, Nakamura S, Clark A, *et al.* Disruption of the transmembrane dense core vesicle proteins IA-2 and IA-2β causes female infertility. *Endocrinology* 2006; 147: 431–438.
12. Nishimura T, Kubosaki A, Ito Y, *et al.* Disturbances in the secretion of neurotransmitters in IA-2/IA-2beta null mice: changes in behavior, learning and lifespan. *Neuroscience* 2009; 159: 427–437.
13. Kim SM, Power A, Brown TM, *et al.* Deletion of the secretory vesicle proteins IA-2 and IA-2beta disrupts circadian rhythms of cardiovascular and physical activity. *FASEB J* 2009; 23: 3226–3232.

BJP British Journal of Pharmacology

DOI:10.1111/j.1476-5381.2012.01853.x
www.brjpharmacol.org

RESEARCH PAPER

Loss of multidrug and toxin extrusion 1 (MATE1) is associated with metformin-induced lactic acidosis

K Toyama[1], A Yonezawa[1], S Masuda[1], R Osawa[1], M Hosokawa[2], S Fujimoto[2], N Inagaki[2], K Inui[1,3] and T Katsura[1]

[1]*Department of Pharmacy, Kyoto University Hospital, Faculty of Medicine, Kyoto University, Kyoto, Japan,* [2]*Department of Diabetes and Clinical Nutrition, Graduate School of Medicine, Kyoto University, Kyoto, Japan, and* [3]*Kyoto Pharmaceutical University, Kyoto, Japan*

Correspondence
Toshiya Katsura, Department of Pharmacy, Kyoto University Hospital, Sakyo-ku, Kyoto 606-8507, Japan. E-mail: tkatsura@kuhp.kyoto-u.ac.jp

Keywords
H^+/organic cation antiporter; genetic variant; toxicodynamics; kidney; liver

Received
24 August 2011
Revised
5 December 2011
Accepted
5 January 2012

BACKGROUNDS AND PURPOSE

Lactic acidosis is a fatal adverse effect of metformin, but the risk factor remains unclear. Multidrug and toxin extrusion 1 (MATE1) is expressed in the luminal membrane of the kidney and liver. MATE1 was revealed to be responsible for the tubular and biliary secretion of metformin. Therefore, some *MATE* polymorphisms, that cause it to function abnormally, are hypothesized to induce lactic acidosis. The purpose of this study is to clarify the association between *MATE* dysfunction and metformin-induced lactic acidosis.

EXPERIMENTAL APPROACH

Blood lactate, pH and bicarbonate ion (HCO_3^-) levels were evaluated during continuous administration of 3 $mg \cdot mL^{-1}$ metformin in drinking water using *Mate1* knockout (–/–), heterozygous (+/–) and wild-type (+/+) mice. To determine the tissue accumulation of metformin, mice were given 400 $mg \cdot kg^{-1}$ metformin orally. Furthermore, blood lactate data were obtained from diabetic patients given metformin.

KEY RESULTS

Seven days after metformin administration in drinking water, significantly higher blood lactate, lower pH and HCO_3^- levels were observed in *Mate1*$^{-/-}$ mice, but not in *Mate1*$^{+/-}$ mice. The blood lactate levels were not affected in patients with the heterozygous *MATE* variant (*MATE1*-L125F, *MATE1*-G64D, *MATE2-K*-G211V). Sixty minutes after metformin administration (400 $mg \cdot kg^{-1}$, p.o.) the hepatic concentration of metformin was markedly higher in *Mate1*$^{-/-}$ mice than in *Mate1*$^{+/+}$ mice.

CONCLUSION AND IMPLICATIONS

MATE1 dysfunction caused a marked elevation in the metformin concentration in the liver and led to lactic acidosis, suggesting that the homozygous *MATE1* variant could be one of the risk factors for metformin-induced lactic acidosis.

Abbreviations

ALT, alanine aminotranferase; AST, aspartate aminotransferase; BUN, blood urea nitrogen; MATE, multidrug and toxin extrusion; MPP, 1-methyl-4-phenylpyridinium; OCT, organic cation transporter

Introduction

Metformin (*N,N*-dimethylbiguanide) is widely used in the treatment of type II diabetes mellitus. It exhibits pharmacological effects in the liver and is almost entirely excreted in urine in an unchanged form (Scheen, 1996). Lactic acidosis is a fatal adverse effect of biguanide agents including metformin (Bailey and Turner, 1996). It was reported that metformin-induced lactic acidosis was associated with an elevation in plasma concentrations of metformin in patients

with renal failure (Pearlman *et al.*, 1996; Safadi *et al.*, 1996). However, it is noteworthy that metformin-induced lactic acidosis also occurs in patients without any risk factors (Tymms and Leatherdale, 1988; al-Jebawi *et al.*, 1998; Misbin *et al.*, 1998). These reports suggest that some risk factors in addition to renal impairment are associated with metformin-induced lactic acidosis.

Multidrug and toxin extrusion 1 (MATE1/SLC47A1) is expressed in the luminal membranes of renal proximal tubules and bile canalicular membranes of hepatocytes and is responsible for the efflux of cationic compounds, including metformin, from the cells (Otsuka *et al.*, 2005; Yonezawa and Inui, 2011). In the basolateral membranes of liver and kidney, organic cation transporters, OCT1 (SLC22A1) and OCT2 (SLC22A2), mediate metformin uptake from blood into cells respectively (Wang *et al.*, 2003; Kimura *et al.*, 2005). The renal clearance of metformin is five times higher than the glomerular filtration rate (Scheen, 1996), suggesting that the vectorial secretion via basolateral OCT2 and luminal MATE is important for the urinary excretion of metformin. Previously, we have demonstrated that the pharmacokinetics of metformin was significantly changed in *Mate1* knockout (*Mate1*$^{-/-}$) mice (Tsuda *et al.*, 2009). It was shown that the total body clearance and renal clearance was decreased to 25% and 18% in comparison with the wild-type (*Mate1*$^{+/+}$) mice, respectively. Therefore, it is thought that MATE1 determines the pharmacokinetics of metformin.

Transporter function is associated with inter-individual variations in drug responses. A *MATE1* rs2289669G>A variant located in the intron region was reported to be related to a glucose-lowering effect after metformin treatment in patients with diabetes, although little is known about the influence of the molecular mechanism of this variant on the MATE1 transporter (Becker *et al.*, 2009). In addition, it was reported that metformin elevates the blood lactate level in the presence of the MATE1 inhibitor pyrimethamine in mice, but under the conditions where the plasma concentration of metformin is much higher than those found in clinical situations (Ito *et al.*, 2010). These reports suggested that MATE1 function influenced the pharmacodynamics of metformin under these limited conditions. Previously, we and other groups have identified non-synonymous *MATE* variants with reduced or negligible transport activity (Chen *et al.*, 2009; Kajiwara *et al.*, 2009; Meyer zu Schwabedissen *et al.*, 2010). Taken together, these data indicate that functional impairment of MATE1 such as occurs with the genetic polymorphisms is involved in the lactic acidosis caused by metformin.

Here, we examined whether dysfunctional MATE1 caused metformin-induced lactic acidosis by using *Mate1* knockout mice as models of *MATE* variant carriers. In addition, we also investigated the effect of heterozygous *MATE* variants on blood lactate levels after metformin treatment both in mice and in humans. Our results indicated that MATE dysfunction is one of the risk factors for metformin-induced lactic acidosis.

Methods

Animals

Animals used in the present study were male C57BL/6 *Mate1*$^{+/+}$, *Mate1*$^{+/-}$ and *Mate1*$^{-/-}$ mice between 10 and 17 weeks of age. The methods used to generate the *Mate1* knockout mice were described previously (Tsuda *et al.*, 2009). In the present study, 6–12 mice were used in each experiment. Mice were kept in a temperature-controlled environment with a 14 h light and 10 h dark cycle, and received a standard diet and water *ad libitum*. All animal care and experimental procedures were conducted in accordance with *The Guidelines for Animal Experiments of Kyoto University*. All protocols were approved by the Animal Research Committee, Graduate School of Medicine, Kyoto University.

Long-term oral administration of metformin in mice

Mice (*Mate1*$^{+/+}$, $n = 9$; *Mate1*$^{+/-}$, $n = 9$; *Mate1*$^{-/-}$, $n = 11$) were given 3 mg·mL^{-1} metformin in drinking water for 21 days. One to four mice were kept in the same cage. The total volume of drinking water in each cage was measured at days 7, 14 and 21 to calculate the mean daily dosage of metformin. For blood collection, the mice were deprived of food (fasted) for 4 h before being anaesthetized with sodium pentobarbital (50 mg·kg^{-1} i.p.). Blood samples were collected from the tail vein, under 40 min of anaesthesia, before and at 7, 14 and 21 days after the administration of metformin. Blood lactate, pH and bicarbonate ion (HCO_3^-) levels were measured by an i-STAT analyser with a CG4+ cartridge (Fuso Pharmaceutical Industries, Osaka, Japan). Body weight was also measured at the same time. At the end of this experiment, blood samples were collected from the abdominal aorta, and aspartate aminotransferase (AST), alanine aminotranferease (ALT), blood urea nitrogen (BUN) and plasma creatinine levels were determined.

Single oral administration of metformin in mice

Mice were given 5 mL·kg^{-1} water (*Mate1*$^{+/+}$, $n = 6$; *Mate1*$^{-/-}$, $n = 7$) or 400 mg·kg^{-1} metformin (*Mate1*$^{+/+}$, $n = 7$; *Mate1*$^{-/-}$, $n = 12$) via oral gavage under 40 min of anaesthesia. To determine the baseline lactate level, blood samples were obtained by tail bleeding before the oral administration of metformin. At 24 h after oral administration, blood lactate levels and plasma concentrations of metformin were determined using blood samples obtained from the tail vein. Blood lactate levels were measured by Lactate Pro LT-1710 (Arkray Inc., Kyoto, Japan). At the end of this experiment, blood samples were collected from the abdominal aorta, and biochemical parameters were evaluated by i-STAT analyser with CG4+ and CHEM8+ cartridges (Fuso). Thereafter, mice were killed, and samples of the kidney, liver and skeletal muscle were obtained.

Metformin and lactate concentration–time profile in Mate1 knockout mice

Mate1$^{-/-}$ mice ($n = 8$) were deprived of food for 12 h before the administration of 150 mg·kg^{-1} metformin via oral gavage. Blood samples were obtained from the tail vein as before and at 0.5, 1, 2, 4 and 8 h after the oral administration metformin to measure blood lactate levels and plasma concentrations of metformin. Blood lactate levels were measured by Lactate Pro (Arkray).